EasyChair Preprint

№ 9638

Simulation of the Secondary Neutrons Production in a Soft Tissue Phantom Produced by Protons and Carbon Ions: Utilizing the PHITS Monte Carlo Code for a Comparative Study

Mohamed El-Asery, Zouhair Sadoune, Hassane El Bekkouri, Adil Bardane, Abdessamad Didi, El Mehdi Alibrahimi and Chakir El Mahjoub

January 30, 2023

Simulation of the secondary neutrons production in a soft tissue phantom produced by protons and carbon ions: Utilizing the PHITS Monte Carlo Code for a Comparative Study

Mohamed El-asery
Dept. of Physics Faculty of f Science
Ibn Tofail University
Kenitra, Morocco
mohamed.el-asery@uit.ac.ma

Zouhair Sadoune
Dept. of Physics Faculty of Science
Ibn Tofail University
Kenitra, Morocco
zouhair.sadoune@uit.ac.ma

Hassane El bekkouri
Dept. of Physics Faculty of Science
Ibn Tofail University
Kenitra, Morocco
hassane.elbekkouri@uit.ac.ma

Adil Bardane
Dept. of Physics Faculty of Science
Ibn Tofail University
Kenitra, Morocco
adil.bardane@usmba.ac.ma

Abdessamad Didi
Dept. of Physics, Faculty of Science
Mohammed First University
Oujda, Morocco
a.didi@ump.ac.ma

El mehdi Al ibrahimi
Dept. of Physics Faculty of Science
Ibn Tofail University
Kenitra, Morocco
alibrahmi.elmehdi@uit.ac.ma

Chakir El mahjoub
Dept. of Physics Faculty of Science
Ibn Tofail University
Kenitra, Morocco
elmahjoub.chakir@uit.ac.ma

***Abstract*—Hadron therapy (HT) is a technique that often uses accelerated ions to destroy tumors, such as protons and carbon ions, and is highly successful for some radiation-resistant cancers. Despite the fact that most of the dose in HT is delivered to the tumor volume through electromagnetic interactions with atomic electrons which allows for excellent dose distributions, consequently, tumors located near critical organs become the indicator of choice compared to photon radiotherapy. However, the nuclear reactions induced by the primary particles can generate undesirable secondary radiation interactions. As a result, a significant portion of the patient's body may be exposed to the secondary background radiation field which increases the secondary cancer risk, particularly relevant for pediatric or re-irradiated patients. Thus, these unwanted secondary particles should be evaluated. The purpose of this research is to evaluate the dose of protons and carbon ions by measurements of dose distributions of secondary particles especially those produced in the patient's tissue by using two energies 135 MeV proton, and 264 MeV/u carbon ions beam((^{12}C)) in a soft tissue phantom. The Bragg peak position and dose distribution were compared. We used for this research the Monte Carlo radiation transport code, called Particle and Heavy Ion Transport code System (PHITS).**

***Index Terms*—Hadron therapy, dose, nuclear reactions, secondary radiation, secondary cancer risk, Bragg peak.**

I. Introduction

Hadron Therapy (HT) is an emerging technique in the treatment of cancerous tumors such as those that are difficult to access by surgery or cancers located near sensitive structures or difficult to cure with other forms of treatment [1]–[3]. The principle consists of the use of light ion or proton beams to locally irradiate cancerous tumors because of their physical and biological effectiveness. Protons have unquestionable ballistic advantages (due to energy losses during interactions). The energy deposit per unit length increases until the particle stops. Thus, the energy deposition is higher at the end of the trajectory: this is the Bragg peak (BP). The existence of this peak greatly improves the ratio between the radiation dose at the tumor level and that deposited in healthy tissue [4], [5].
The relative biological efficiency of protons is close to that of photons and varies with the depth and energy of the incident protons.
The use of carbon ions in the treatment of tumors is based on these two advantages:
- A ballistic advantage, allowing precision irradiation. Due to their high mass, their lateral dispersion is lower than that of protons and not very dependent on tissue depth.
- A higher relative biological efficiency (RBE) than protons, and photons: the region of highest RBE values are located at the end of the particle path, as well lower "Oxygen Enhancement Ratio". These radiobiological properties enable the use of these ions in radiotherapy to increase its effectiveness.
During the interaction of particles/matter, electronic interactions are the most dominant process, these contribute to the major part of energy deposition.

Charged particles also undergo nuclear inelastic interactions with the nuclei of the crossed medium atoms creating gamma rays, charged and neutral secondary particles, result in a non-negligible extra dose being stored in the tumor and surrounding tissues, particularly, neutrons because they have the ability to transport energy far from the treated area and raise the possibility of subsequent cancer years after treatment [6].
Characterizing Secondary Neutron Production (SNP) as a result of primary particle interactions with human tissue is essential for the use of charged particles in radiation treatment. The detector or techniques like Monte Carlo (MC) simulation can find the SNP.
To improve dose predictions, several MC simulation codes are used in proton treatment facilities [7]–[11]. In proton treatment, energy distributions in phantoms with various characteristics and geometries are compared using the GEANT4 and MCNPX MC programs, [11]–[13]. The ideal beam parameters for proton treatment can be found using MC codes like FLUKA, GATE, and PHITS [9]. The GEANT4 MC code was used to determine the energy distribution of monoenergetic neutrons at various depths in tissue-like targets [10]. The PHITS MC code was used to study the interaction between the biological impacts of neutrons and their field properties [7]. To compute the neutron dose, the cross sections of neutron generation by protons with energies of 135 MeV and 180 MeV were calculated. Scintillation detectors have been used in numerous investigations to determine the angular and energy distributions of SNP as a result of bombarding targets of various thicknesses with He ions in a certain energy range [14]–[19]. The flux of secondary neutrons at various angles to the forward direction of the ions was computed by bombarding several targets with He ions in the HIMAC facility and compared with previously published experimental data and the MCNPX MC code [20]. In our study, two energies 140 MeV proton, and 264 MeV/u ^{12}C beam in a soft tissue phantom were studied using a Monte Carlo program code. The PHITS MC simulation was used to evaluate the secondary neutron dose produced by the protons and carbon ions in the medium like the target made by soft tissues, and their contribution to the total dose certainly in the region distal to the BP. The effects of secondary neutrons should be researched in order to protect patients and personnel from radiation. Neutrons are particles that need special attention because of their physical and biological properties. Moreover, determine the total number of SNP delivered by proton and carbon ions, as well as.

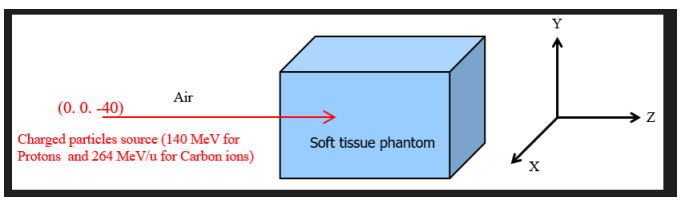

Fig. 1. The geometry used in this simulation.

II. MATERIALS AND METHODS

In this study we use the Monte Carlo particle transport simulation code PHITS [21]. The PHITS code has become an essential tool used in various fields of physics, including the design of radiation protection, nuclear installations, radiation in space, geoscience, and radiotherapy. Developed by the Japan Atomic Energy Agency(JAEA) that allows simulation of the transport of most particles such as neutrons, protons, heavy ions, photons, and electrons... with energy levels up to 1 TeV (per nucleon for ion). Using various nuclear reaction models and data libraries. The Intra-nuclear cascade of the Liège model (INCL 4.6) is used to simulate the nuclear reactions induced by nucleons and light ions [22]. For carbon ions in the range energy (10 MeV/n - 3 GeV/n), PHITS uses several entry models, but only two are suitable. the JAERI Quantum Molecular Dynamics model (JQMD) and its new version JQMD-2.0, and the reaction cross-section model Kurotama was adopted [23]. The Generalized Evaporation Model (GEM) simulates the statistical evaporation of light particles ($Z \leq 12$) and the fission of heavy nuclei ($A \geq 70$) [24]. The energy loss of protons and ions in materials is computed using ATIMA, a tool for stopping power (http://web-docs.gsi.de/ weick/atima/ATIMA website). The JENDL-4.0 nuclear data library for the calculation of the transport of neutrons less than 20 MeV and the emission of secondary particles induced by these neutrons [25]. For neutrons exceeding 20 MeV nuclear reaction models are utilized.
In this study, we simulated a mono-energetic beam, and two different energies were considered: 135 MeV proton beam and 264 MeV/u carbon ions beam. The beam 0.2 cm in diameter, is directed along the z-axis. The primary particles moved through the air at 40 cm and perpendicularly struck the base center of the phantom $20 * 20 * 40 cm^3$ made of soft tissues. There are four components to the soft tissue: oxygen (0.762), carbon (0.111), hydrogen (0.10), and nitrogen (0.026). Figure 1 shows the simulation geometry.
The absorbed dose due to all components (primary particles, secondary charged particles, neutrons) was evaluated in the target volume "Tally" prediction functions such as **Deposit-Tally** which is the energy loss of the charged particles and nucleus, and the absorbed energy is given in (Gy/Source, MeV/Source).

III. RESULTS

In this study, we have carried out simulations for the model shown in Figure 1 with a mesh of a step of 0.1mm in depth all along 40 cm. The number of simulation history is 10^7 particles for protons and 10^6 particles for the ^{12}C. Figure 2 shows the dose distribution in depth. From the results found, we concluded that to reach a target volume located at a depth of about 13.7 cm, the energy of 140 MeV for protons, and 264 MeV/u for ^{12}C are required.
Protons and carbon ions have a physical advantage over X-ray beams because of the tiny peak that appears just before the particles come to a stop Bragg peak. An extremely high and narrow peak is produced at the path's end due to an increase

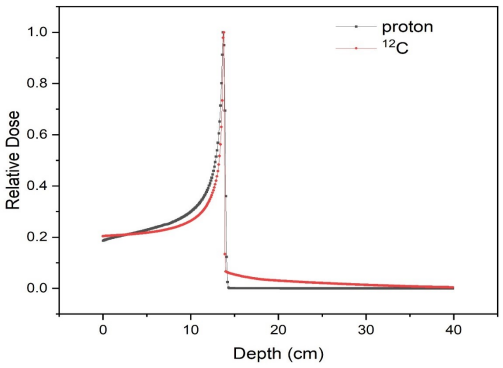

Fig. 2. Depth dose distribution obtained with PHITS for 140MeV proton beam, and 264 MeV/u ^{12}C beam. Data normalized to one source particle.

in deposition energy. For large tumors, The Spread out Bragg Peak (SOBP) is created by combining a number of Bragg peaks that are produced at various depths to cover the tumor size.

The difference between the values represented by the two curves is mostly beyond the Bragg peak. No considerable energy deposition was observed after the Bragg peak (BP) for protons. In the case of carbon ions, different fragments are produced in a phantom. Nuclear reactions along the way decrease the number of primary ions in the beam. These effects are more and more important as the beam penetrates the phantom and finally, the carbon ions are totally attenuated at the Bragg peak. The existence of light fragments after the Bragg peak is due to the fact that the charged fragments produced have an atomic number lower than 6, so their path will be longer. They will then produce a "tail" of dose deposition beyond the Bragg peak. Tail lengths ranged until 16 cm for 264 MeV/u. Before the BP, as expected, carbon ions undergo minor beam broadening compared to protons, allowing precision irradiation. Because of their high mass.

In this study, particular attention was focused on neutrons. They were generated by the interactions of the primary particles in the soft tissue phantom.

To estimate the neutron dose, the deposition energy of the neutrons and secondary charged particles produced by primary particles was estimated using the "tally" function implemented in the PHITS code **counter**. The results are shown in Figure 3, 4.

It is seen that the secondary neutrons produced by primary protons contribute just a minor portion in the Bragg peak. However, after the Bragg peak their contribution is nearly 100%, but in relation to the peak maximum their contribution did not reach 0.01%. The contributions of other secondaries, such as deuterons, 3He, and tritons, are much shorter, Figure 3. For ^{12}C, we noted that the dose deposited before the Bragg peak is mostly attributable to primary carbon ^{12}C, whereas the dose attributable to secondary particles is relatively little. The dose deposited following the Bragg peak is exclusively caused by secondary particles.

The secondary particles contribute a little portion of the overall dose in all overall plateau regions. In the peak maximum more than 90% was deposited by primary ^{12}C vs. 9.28% of the dose deposited by the secondary particles. However, after the Bragg peak, the contributions of the secondary became more significant and represent about 100%.

As seen in Figure 4, the fragments produced are the primary cause of the Bragg peak. They have the longest range and therefore contribute to the long energy deposition tail up to 16 cm.

Secondary neutrons are also created, but these have a much longer path than the other particles and contribute relatively little to the dose Figure 4. However, they made a relatively minor contribution compared to the peak, which was less than 0.1%.

From the result, we conclude that the contribution of the secondary neutron in carbon ions is much more than that of protons by a factor of 10 in the BP. After the BP we see that their contribution represents 0.1% to the BP (peak maximum) and their range is very long compared to other charged particles created.

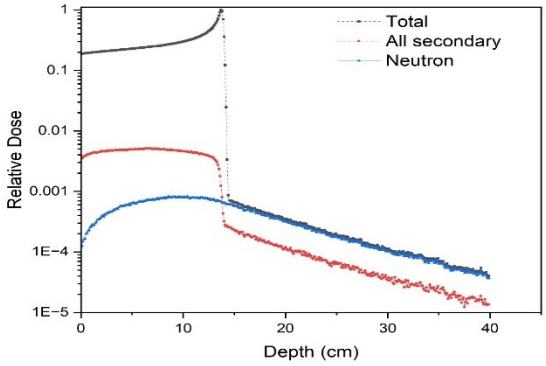

Fig. 3. Relative depth dose distribution for secondary particles and neutrons for proton energy of 140 MeV.

As we know, the fraction of the secondary neutron dose is a function of the total neutrons generated by the interactions, therefore we also performed a simulation to measure the number of secondary neutrons produced (SNP) in the phantom. The production of neutrons as a function of initial proton energy is seen in Figure 5. It is evident that when beam energy is increased, productivity rises. It was observed that our results exceeded those of the research utilizing the GEANT4 code by a factor of 2 [26] and by a factor of 3 with the MCNP code [27]. This disagreement results from a variety of variables, including the various physics models used in each code and the material compositions of each target.

Many studies were made on this subject for particle therapy irradiation [28]. Found using Slab head phantom in the 50-

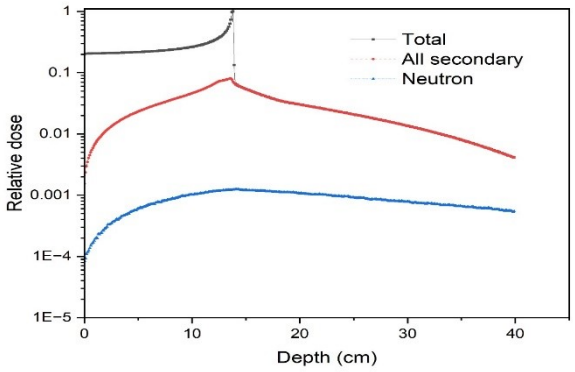

Fig. 4. Relative depth dose distribution for secondary particles and neutrons for ^{12}C with energy of 264 MeV/u.

100 MeV/u range that the number of SNP for alpha particles compared to proton beams increased 7-14 times it is also found in the water phantom for 100 MeV incoming proton energy with the PHITS MC Program 0.051 neutrons per 100 MeV. We got 0.09 neutrons per incoming 100 MeV proton with the same code as PHITS MC.

The biggest difference between ions when comparing energy loss is due to stopping power, which is dependent on the square of the projectile charge. As a result, heavier ions traveling at the same speed suffer a significant increase in energy loss. As a result, the energy loss for carbon ions is 36 times more than it is for protons with the same energy per nucleon.

In terms of therapy, comparing various ions at the same range is more pertinent than doing so at the same energy, which adds another dependent on the velocity. The variety of ions that can exist at a given energy per nucleon scales roughly with $R{\sim}\mathrm{m/z}^2$. As a result, carbon ions have a range that is one-third that of protons at the same energy per nucleon, while helium ions have the same range as protons at the same energy per nucleon. Then we did another simulation to contrast the impact of SNP by proton and ^{12}C for various energies, but they both fell within the same range for two of them. Neutron counts produced by the PHITS simulation are plotted in Figure 6.

The results shown in Figure 6 reported that as the atomic number of the incident particle increases, the number of SNP increases which is in good agreement with the literature [29]. However, the number of SNP of ^{12}C compared to proton beams increased 20 times.

Chaudri found by Monte Carlo simulation a minimum of 4 neutrons of energy above 5 MeV are created for each 400 MeV/u ^{12}C incident energy on the tissue; this number drops to 3, 1.4, and 0.3 for 300, 200, and 100 MeV/u respectively. We got 6.89 neutrons without any restriction energy for 385 MeV/u [30].

Another simulation was carried out to assess secondary neutron energy spectra produced by protons and carbon ions of incoming energy of 140 and 264 MeV/u respectively on a soft tissue phantom. Figure 7. Secondary neutrons have a broad energy spectrum, ranging from low-energy to high-energy neutrons. Target nuclei produce low-energy neutrons, which deposit their energies over relatively small distances. Additionally, when the projectile evaporates, high-energy neutrons are released with a low fluency and deposit their energies across a large area.

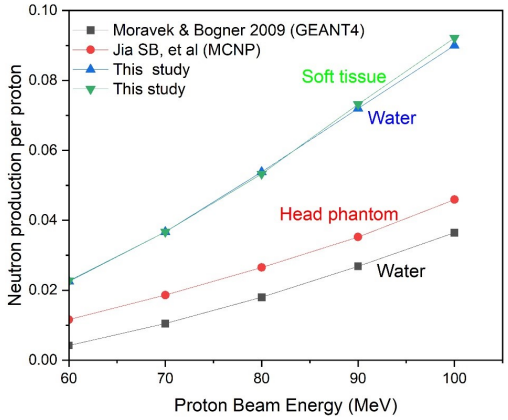

Fig. 5. Secondary neutron generation versus incoming proton energy in a soft tissue phantom in comparison with the literature [26], [27].

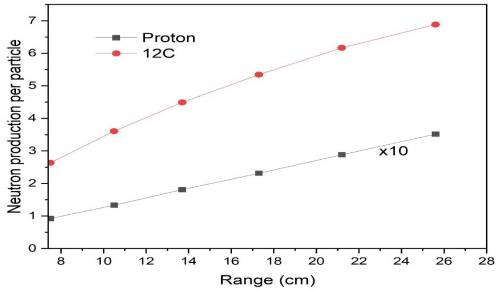

Fig. 6. Secondary neutron generation versus a range of protons and ^{12}C ions in a soft tissue phantom.

IV. DISCUSSION

In this study, we carried out a comparative analysis to examine the particles generated by nuclear interactions between protons and carbon ions in a soft tissue phantom. we observed that the secondary particles, including the neutrons created by primary protons, contributed only a very little amount to the Bragg peak and that their contributions beyond the peak did not exceed 0.01% in relation to the peak maximum. For carbon ions, more than 90% of the dose at the peak maximum was laid down by primary ^{12}C, compared to 9.28% by all secondary particles. Nevertheless, following the Bragg peak, the contributions of the secondary became more significant

and represented 100%, entirely from the contribution of the fragment ions produced by nuclear reactions. Among all the fragments, H and He was the highest, they have the longest range and extend around 16 cm beyond the Bragg peak, and therefore they contribute to the long energy deposition tail, while heavier fragments such as B, Be, Li and secondary carbons ions contribute to the dose more locally.

The neutron contribution to the total dose at the peak maximum represents more than 0.1%, which is significantly more than the neutron contribution from protons to the BP by a factor of 10.

we also performed a simulation to measure the number of secondary neutrons produced (SNP) in the phantom for the protons and carbon ions at the same range of 7.5-26 cm. The results reported that as the atomic number of the incident particle increases, the number of SNP increases which is in good agreement with the literature. However, the number of SNP of ^{12}C compared to proton beams increased 20 times.

Finally, the studies show that secondary neutron energy spectra produced by protons and carbon ions of incoming energy of 140 and 264 MeV/u respectively on a soft tissue phantom have a peak at low energies because target nuclei produce low-energy neutrons, which deposit their energies over relatively small distances. Additionally, high-energy neutrons are released with a low fluency as the projectile evaporates, depositing their energies over a large region.

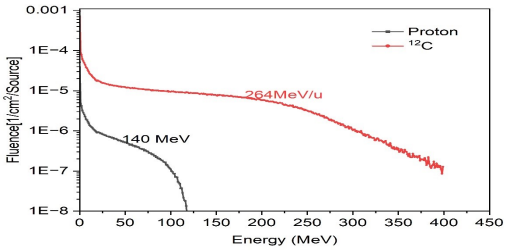

Fig. 7. Induced neutron spectrum derived from 140 MeV of the incident proton beam in comparison with 264 MeV/u ^{12}C ion beam inside the soft tissue phantom.

V. Conclusions

In this research, we used the PHITS to investigate the effect of secondary neutrons and other fragments in the soft tissue phantom. We found that the vast majority is deposited in the tissue via electromagnetic interactions with atomic electrons, allowing for excellent dose distributions. However, the nuclear reactions induced by the protons and carbon ions can generate undesirable secondary radiation. We noticed that the secondary particles were created, and SNP rises as the atomic number of the incident particle increased, which is in good accord with the literature. Therefore, it was observed that these particles with other fragments are responsible for the dose deposition after the Bragg peak. Secondary neutrons contribute 90% to the total depth dose deposition behind the BP produced by protons, Further on, it shows that the dose of secondary neutrons produced by protons decreased exponentially with the distance after the BP. It was determined that the neutron contribution created by protons to the dose behind the BP was at least 0.01%, Consequently, it does not seem that the neutrons produced by the interactions between the protons pose a substantial risk to the patient's body throughout the treatment procedure. For ^{12}C, Just behind the Bragg peak, the total depth dose deposition contributes 100%. Neutrons make up more than 0.1% of the secondary particle field. However, the neutrons created by ^{12}C travel farther away behind the BP up to 20 cm. As a result, a significant portion of the patient's body may be exposed to secondary background radiation. This dose, although low, can nevertheless still be an issue if the tumor is close to particularly sensitive organs in a longitudinal direction field which increases the secondary cancer risk, which is particularly relevant for pediatric or re-irradiated patients. Thus, these unwanted secondary particles are being addressed by medical physicists.

Acknowledgment

Thank you to all researchers in the Electronic Systems, Information Processing, Mechanics, and Energy Laboratory. From them. I learned a lot about life in general and about scientific research and received a lot of personal and professional advice. I would also like to thank the director of the Center for Computational Science & E-Systems at the Japan Atomic Energy Agency (JAEA) for allowing me to use the PHITS (Particle and Heavy Ion Transport System) code.

References

[1] Marco Durante, Francis A Cucinotta, and Jay S Loeffler. Charged particles in oncology, 2017.

[2] Timothy D Malouff, Anita Mahajan, Sunil Krishnan, Chris Beltran, Danushka S Seneviratne, and Daniel Michael Trifiletti. Carbon ion therapy: a modern review of an emerging technology. *Frontiers in oncology*, 10:82, 2020.

[3] Marco Durante and Jürgen Debus. Heavy charged particles: does improved precision and higher biological effectiveness translate to better outcome in patients? In *Seminars in radiation oncology*, volume 28, pages 160–167. Elsevier, 2018.

[4] Gerhard Kraft. Tumor therapy with heavy charged particles. *Progress in particle and Nuclear Physics*, 45:S473–S544, 2000.

[5] Anthony Zietman. Proton beam and prostate cancer: an evolving debate. *Reports of Practical Oncology and Radiotherapy*, 18(6):338–342, 2013.

[6] E Gioscio, G Battistoni, A Bochetti, M De Simoni, Y Dong, M Fischetti, I Mattei, R Mirabelli, S Muraro, V Patera, et al. Development of a novel neutron tracker for the characterisation of secondary neutrons emitted in particle therapy. *Nuclear Instruments and Methods in Physics Research Section A: Accelerators, Spectrometers, Detectors and Associated Equipment*, 958:162862, 2020.

[7] G Baiocco, S Barbieri, G Babini, J Morini, D Alloni, W Friedland, P Kundrát, E Schmitt, M Puchalska, L Sihver, et al. The origin of neutron biological effectiveness as a function of energy. *Scientific reports*, 6(1):1–14, 2016.

[8] Tsuyoshi Kajimoto, Kenichi Tanaka, Satoru Endo, So Kamada, Hiroki Tanaka, Masashi Takada, and Tsuyoshi Hamano. Double differential cross sections of neutron production by 135 and 180 mev protons on a-150 tissue-equivalent plastic. *Nuclear Instruments and Methods in Physics Research Section B: Beam Interactions with Materials and Atoms*, 487:38–44, 2021.

[9] Keita Kurosu, Masaaki Takashina, Masahiko Koizumi, Indra J Das, and Vadim P Moskvin. Optimization of gate and phits monte carlo code parameters for uniform scanning proton beam based on simulation with fluka general-purpose code. *Nuclear Instruments and Methods in Physics Research Section B: Beam Interactions with Materials and Atoms*, 336:45–54, 2014.

[10] Christopher M Lund, G Famulari, L Montgomery, and J Kildea. A microdosimetric analysis of the interactions of mono-energetic neutrons with human tissue. *Physica Medica*, 73:29–42, 2020.

[11] U Titt, B Bednarz, and H Paganetti. Comparison of mcnpx and geant4 proton energy deposition predictions for clinical use. *Physics in Medicine & Biology*, 57(20):6381, 2012.

[12] Abdessamad Didi, Hassane Dekhissi, Rajaa Sebihi, Mustapha Krim, and Reda Mesradi Mohamed. Calculate primary and secondary dose in proton therapy using 200 and 250 mev proton beam energy. *Moscow University Physics Bulletin*, 74(4):364–368, 2019.

[13] El-Asery Mohamed, Sadoune Zouhair, El Bekkouri Hassane, Didi Abdessamad, and Chakir El Mahjoub. Evaluation of secondary neutron produced in proton therapy using phits. *Moscow University Physics Bulletin*, In Press, 2023.

[14] RA Cecil, BD Anderson, AR Baldwin, R Madey, A Galonsky, P Miller, L Young, and FM Waterman. Neutron angular and energy distributions from 710-mev alphas stopping in water, carbon, steel, and lead, and 640-mev alphas stopping in lead. *Physical Review C*, 21(6):2471, 1980.

[15] L Heilbronn, RS Cary, M Cronqvist, F Deak, K Frankel, A Galonsky, K Holabird, A Horvath, A Kiss, J Kruse, et al. Neutron yields from 155 mev/nucleon carbon and helium stopping in aluminum. *Nuclear science and engineering*, 132(1):1–15, 1999.

[16] L Heilbronn, CJ Zeitlin, Y Iwata, T Murakami, H Iwase, T Nakamura, T Nunomiya, H Sato, H Yashima, RM Ronningen, et al. Secondary neutron-production cross sections from heavy-ion interactions between 230 and 600 mev/nucleon. *Nuclear science and engineering*, 157(2):142–158, 2007.

[17] T Kurosawa, N Nakao, T Nakamura, Y Uwamino, T Shibata, N Nakanishi, A Fukumura, and K Murakami. Measurements of secondary neutrons produced from thick targets bombarded by high-energy helium and carbon ions. *Nuclear Science and Engineering*, 132(1):30–57, 1999.

[18] T Kurosawa, T Nakamura, N Nakao, T Shibata, Y Uwamino, and A Fukumura. Spectral measurements of neutrons, protons, deuterons and tritons produced by 100 mev/nucleon he bombardment. *Nuclear Instruments and Methods in Physics Research Section A: Accelerators, Spectrometers, Detectors and Associated Equipment*, 430(2-3):400–422, 1999.

[19] H Sato, T Kurosawa, H Iwase, T Nakamura, Y Uwamino, and N Nakao. Measurements of double differential neutron production cross sections by 135 mev/nucleon he, c, ne and 95 mev/nucleon ar ions. *Physical Review C*, 64(3):034607, 2001.

[20] Pedro Ortego. Benchmarking of mcnpx with the experimental measurements of high-energy helium ions in himac facility. *Radiation protection dosimetry*, 116(1-4):43–49, 2005.

[21] Tatsuhiko Sato, Yosuke Iwamoto, Shintaro Hashimoto, Tatsuhiko Ogawa, Takuya Furuta, Shin-ichiro Abe, Takeshi Kai, Pi-En Tsai, Norihiro Matsuda, Hiroshi Iwase, et al. Features of particle and heavy ion transport code system (phits) version 3.02. *Journal of Nuclear Science and Technology*, 55(6):684–690, 2018.

[22] Alain Boudard, Joseph Cugnon, J-C David, Sylvie Leray, and Davide Mancusi. New potentialities of the liège intranuclear cascade model for reactions induced by nucleons and light charged particles. *Physical Review C*, 87(1):014606, 2013.

[23] Kei Iida, Akihisa Kohama, and Kazuhiro Oyamatsu. Formula for proton–nucleus reaction cross section at intermediate energies and its application. *Journal of the Physical Society of Japan*, 76(4):044201, 2007.

[24] S Furihata. The gem code-the generalized evaporation model and the fission model. In *Advanced Monte Carlo for Radiation Physics, Particle Transport Simulation and Applications: Proceedings of the Monte Carlo 2000 Conference, Lisbon, 23–26 October 2000*, pages 1045–1050. Springer, 2001.

[25] Keiichi Shibata, Osamu Iwamoto, Tsuneo Nakagawa, Nobuyuki Iwamoto, Akira Ichihara, Satoshi Kunieda, Satoshi Chiba, Kazuyoshi Furutaka, Naohiko Otuka, Takaaki Ohsawa, et al. Jendl-4.0: a new library for nuclear science and engineering. *Journal of Nuclear Science and Technology*, 48(1):1–30, 2011.

[26] Zdenek Morávek and Ludwig Bogner. Analysis of the physical interactions of therapeutic proton beams in water with the use of geant4 monte carlo calculations. *Zeitschrift für Medizinische Physik*, 19(3):174–181, 2009.

[27] Sayyed Bijan Jia, Mohammad Hadi Hadizadeh, Ali Asghar Mowlavi, and Mahdy Ebrahimi Loushab. Evaluation of energy deposition and secondary particle production in proton therapy of brain using a slab head phantom. *Reports of practical oncology and radiotherapy*, 19(6):376–384, 2014.

[28] Adem PEHLİVANLI and Mustafa Hicabi BÖLÜKDEMİR. The effect of proton and helium ions on secondary neutron production in the slab head phantom. *Süleyman Demirel Üniversitesi Fen Edebiyat Fakültesi Fen Dergisi*, 16(2):513–522, 2021.

[29] Irena Gudowska and Nikolai Sobolevsky. Simulation of secondary particle production and absorbed dose to tissue in light ion beams. *Radiation protection dosimetry*, 116(1-4):301–306, 2005.

[30] M Anwar Chaudhri. Neutron production from patients during therapy with bremsstrahlung and hadrons: Are there potential risks with hadrons, especially with carbon ions? In *World Congress on Medical Physics and Biomedical Engineering 2006*, pages 2207–2210. Springer, 2007.